NANO LETTERS

Letter

pubs.acs.org/NanoLett

Conductance Quantization at Zero Magnetic Field in InSb Nanowires

Jakob Kammhuber,[†] Maja C. Cassidy,[†] Hao Zhang,[†] Önder Gül,[†] Fei Pei,[†] Michiel W. A. de Moor,[†] Bas Nijholt,[†] Kenji Watanabe,[‡] Takashi Taniguchi,[‡] Diana Car,[¶] Sébastien R. Plissard,[†,¶,§] Erik P. A. M. Bakkers,[†,¶] and Leo P. Kouwenhoven*[,†]

[†]QuTech and Kavli Institute of Nanoscience, Delft University of Technology, 2628 CJ Delft, The Netherlands

[‡]Advanced Materials Laboratory, National Institute for Materials Science, 1-1 Namiki, Tsukuba 305-0044, Japan

[¶]Department of Applied Physics, Eindhoven University of Technology, 5600 MB Eindhoven, The Netherlands

S Supporting Information

ABSTRACT: Ballistic electron transport is a key requirement for existence of a topological phase transition in proximitized InSb nanowires. However, measurements of quantized conductance as direct evidence of ballistic transport have so far been obscured due to the increased chance of backscattering in one-dimensional nanowires. We show that by improving the nanowire—metal interface as well as the dielectric environment we can consistently achieve conductance quantization at zero magnetic field. Additionally we study the contribution of orbital effects to the sub-band dispersion for different orientation of the magnetic field, observing a near-degeneracy between the second and third sub-bands.

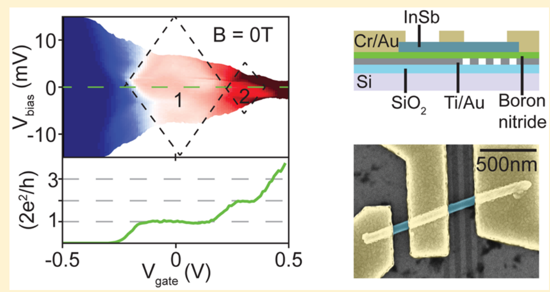

KEYWORDS: *Quantum point contact, conductance quantization, nanowire, InSb, subband, orbital effects*

Semiconducting nanowires made from InAs and InSb are prime candidates for the investigation of novel phenomena in electronic devices. The intrinsic strong spin—orbit interaction (SOI) and large g-factor combined with flexible fabrication has resulted in these materials being investigated for applications in quantum computing,[1−3] spintronics,[4−6] and Cooper pair splitters.[7,8] More recently, these nanowires have been investigated as solid-state hosts for Majorana zero modes (MZMs).[9−12] By bringing a one-dimensional (1D) nanowire with strong SOI into close contact with a superconductor under an external magnetic field, a region with inverted band structure emerges, creating MZMs at its ends. Together with strong SOI and induced superconductivity, a key requirement for MZMs is quasi-ballistic electron transport along the length of the proximitized region in the nanowire, with a controlled odd number of occupied modes.[13] In the absence of scattering, the motion of 1D confined electrons will be restricted to discrete energy bands resulting in quantized conductance plateaus.[14,15] Measurements of quantized conductance in the nanowires therefore provide direct evidence for controlled mode occupation, as well as ballistic transport in these nanowires.

Although now routine in gate defined quantum point contacts (QPC) in two-dimensional electron gases (2DEGs),[14−18] quantized conductance in one-dimensional semiconductor nanowires is more difficult to achieve. In a 1D nanowire, scattering events along the electrons path to and through the constriction between the source and drain contacts have an increased probability of reflection, obscuring the observation of quantized conductance.[19] These scattering events may be due to impurities and imperfections in the crystal lattice or due to surface states that create inhomogeneities in the local electrostatic environment.[20] A Schottky barrier between the nanowire and metallic contacts will result in additional backscattering events, further smearing out the quantized conductance plateaus. To date, quantized conductance in InSb nanowires has only been observed at high magnetic fields (>4 T), where electron backscattering is strongly suppressed.[19] No quantization has been observed in InSb for magnetic fields below 1 T, where the topological transition is expected to take place.[9]

Here we demonstrate conductance quantization in InSb nanowires at zero magnetic field. We have developed a robust fabrication recipe for observing quantized conductance by optimizing both the metal—nanowire contact interface and dielectric environment through the use of hexagonal boron nitride (hBN) as a gate dielectric. We study the evolution of the quantized conductance plateaus with both source-drain bias as well as magnetic field, and extract values for the Landé g-factor of the first three sub-bands in the nanowire. Additionally we study the contribution of orbital effects to the sub-band dispersion for perpendicular magnetic fields.

Figure 1a shows a cross-sectional view of our devices. They consist of an intrinsic Si-substrate with local metallic gates made of Ti/Au (5/10 nm), on top of which a sheet of hexagonal boron nitride (hBN) is mechanically transferred as the

Received: January 5, 2016
Revised: April 11, 2016
Published: April 28, 2016

DOI: 10.1021/acs.nanolett.6b00051
Nano Lett. 2016, 16, 3482−3486

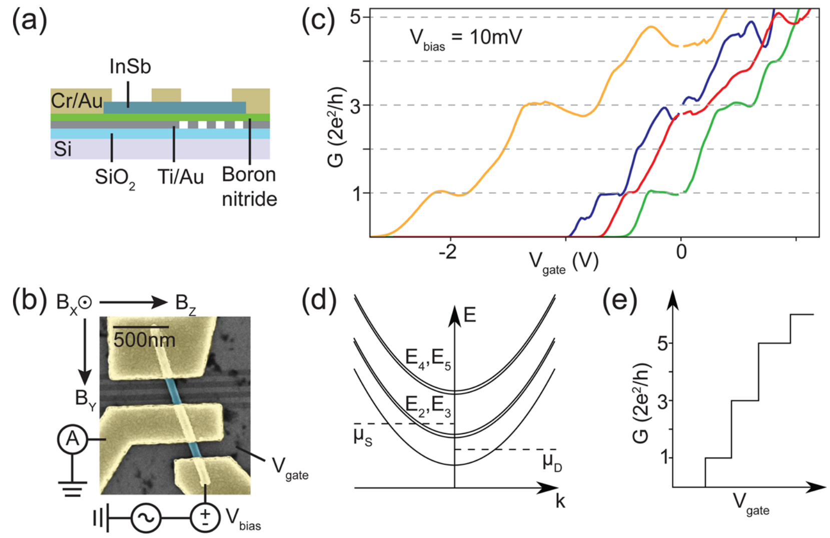

Figure 1. (a) Cross-sectional schematic and (b) false color SEM image of a typical device. An InSb nanowire (blue) contacted by Cr/Au (yellow) is deposited on Ti/Au metal gates (gray) covered with hexagonal boron nitride (green) as insulating dielectric. (c) Pinch-off traces of four different devices each showing quantized conductance plateaus at high bias voltage (V_{bias} = 10 mV). (d) Schematic diagram of the first five sub-bands in a nanowire. At zero magnetic field, each spin-degenerate sub-band below the Fermi level contributes a conductance of $G_0 = 2e^2/h$. Due to the rotational symmetry of the nanowires E_2,E_3 and E_4,E_5 are almost degenerate. (e) Sketch of the expected conductance steps as a function of V_{gate} at high bias voltage showing suppression of the second and fourth plateaus due to orbital sub-band degeneracy.

dielectric. The chemical stability, atomic flatness, and high breakdown voltage,[21] together with the well established dry transfer mechanism[22] makes hBN an ideal dielectric for our nanowire devices. InSb nanowires grown by metal−organic vapor phase epitaxy[23,24] (1−3 μm long and 70−90 nm diameter) are transferred deterministically with a micro-manipulator[25] onto the hBN dielectric. Electrical contacts to the nanowire (evaporated Cr/Au (10/100 nm), 150−400 nm spacing) are defined by electron beam lithography. Before contact deposition, the surface oxide of the nanowires is removed using sulfur passivation[26] followed by a short in situ He-ion mill. Residual sulfur from the passivation step also induces surface doping, which aids contact transparency. Further details of the fabrication are included in the Supporting Information. A top view scanning electron microscope image of a finished device is shown in Figure 1b. The samples are mounted in a dilution refrigerator with a base temperature of 15 mK and measured using standard lock-in techniques at 73 Hz with an excitation V_{RMS} = 70 μV. Voltage is applied to the outer contact and current measured through the grounded central contact, while the third, unused contact is left floating.

We first characterize each device by sweeping the voltage on the underlying gate V_{gate} at fixed bias voltage V_{bias} = 10 mV across the sample. Conductance is obtained directly from the measured current $G = I/V_{\mathrm{bias}}$ and an appropriate series resistance is subtracted in each case (see Supporting Information). Figure 1c plots the conductance of the nanowire as a function of gate voltage for four different devices fabricated on the same chip. Devices with both fine gates as well as wide back gates have been measured. We find that while fine gates allow more flexible gating, devices with wide back gates showed more pronounced conductance plateaus even after extensive tuning of the fine gates. Data from additional devices all fabricated on the same chip is included in the Supporting Information.

As seen in Figure 1c all devices show well-defined plateaus at G_0 and $3G_0$ but the plateaus at $2G_0$ and $4G_0$ appear smaller or even completely absent. Unlike QPCs formed in 2DEGs, nanowires possess rotational symmetry. This symmetry can give rise to additional orbital degeneracies in the energies for the second and third as well as the fourth and fifth sub-band (Figure 1d).[27,28] In conductance measurements at finite bias, sub-bands that are close in energy or degenerate will be populated at similar values in gate voltage giving a double step of $4\frac{e^2}{h}$ instead of $2\frac{e^2}{h}$, which explains the suppressed plateaus at 2 and $4G_0$ (Figure 1e).[29]

To investigate this phenomenon in more detail, we measure the differential conductance $G = \mathrm{d}I/\mathrm{d}V_{\mathrm{bias}}$ as a function of gate voltage and bias voltage for one of these devices (corresponding to the green trace in Figure 1c). This data is shown in Figure 2a as a color plot, with line cuts along 0 and 10 mV bias voltage added in the bottom panel. At zero bias voltage an extended plateau is visible at $1G_0$, together with an additional

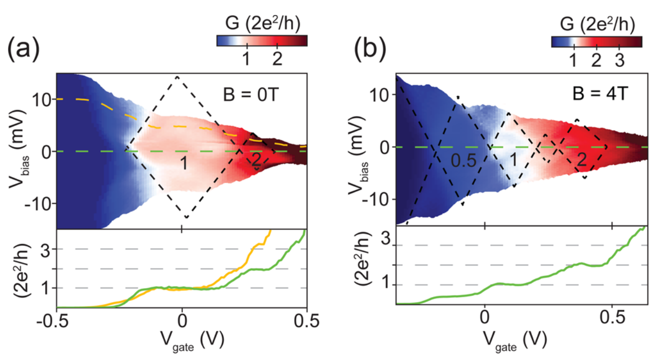

Figure 2. (a) Color-plot of the differential conductance $G = \mathrm{d}I/\mathrm{d}V_{\mathrm{bias}}$ as a function of V_{bias} and V_{gate} at B = 0 T. A line cut along 0 mV (green) and 10 mV (orange) bias voltage is shown in the bottom panel. (b) Differential conductance $G = \mathrm{d}I/\mathrm{d}V_{\mathrm{bias}}$ as a function of V_{bias} and V_{gate} at B_Z = 4 T. An average line cut along 0 ± 0.2 mV bias voltage is shown in the bottom panel. Black dotted lines indicating plateaus of constant conductance are drawn as guide to the eye.

DOI: 10.1021/acs.nanolett.6b00051
Nano Lett. 2016, 16, 3482−3486

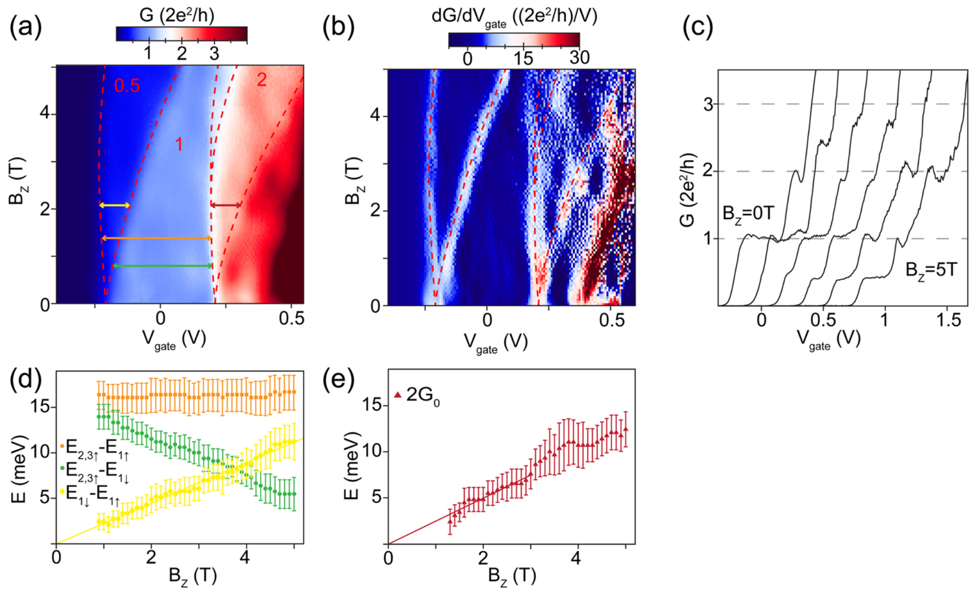

Figure 3. (a) Differential conductance $G = dI/dV_{bias}$ and (b) transconductance dG/dV_{gate} as a function of magnetic field along B_Z and V_{gate} taken at V_{bias} = 0 mV. The level spacings plotted in (d,e) are marked by arrows of corresponding color. Red dashed lines indicating the sub-band spacing in (a,b) are drawn as guide to the eye. (c) Linecuts of (a) in steps of 1T and offset by 200 mV for clarity. (d) Energy level spacings of $E_{1\downarrow} - E_{1\uparrow}$ (yellow), $E_{2,3\uparrow} - E_{1\downarrow}$ (green), and $E_{2,3\uparrow} - E_{1\uparrow}$ (orange) extracted from the 0.5 and 1G_0 plateau in (a). A linear fit to $E_{1\downarrow} - E_{1\uparrow}$ fixed at the origin gives the g-factor of the first sub-band g_1 = 39 ± 1. (e) Energy spacing of $E_{2,3\downarrow} - E_{2,3\uparrow}$ extracted from the 2G_0 plateau with $g_{2,3}$ = 38 ± 1.

small plateau at 2G_0, which is not visible at the high conductance traces. The existence of this small 2G_0 plateau indicates that the device has a small, but finite energy splitting between the second and third sub-band. At finite bias voltage the conductance will only be quantized in integer values of G_0 if both μ_{source} and μ_{drain} occupy the same sub-band. This creates diamond shaped regions of constant conductance indicated by black dotted lines in Figure 2a. At the tip of the diamond the two dotted lines cross when V_{bias} is equal to the sub-band energy spacing $\Delta E_{subband}$. From this we extract $\Delta E_{subband}$ and the lever-arm η of the bottom gate via $\eta V_{gate} = \Delta E_{subband}$.[30] A finite magnetic field breaks time reversal symmetry, lifting spin degeneracy and splitting the individual spin sub-bands $E_{n,\uparrow/\downarrow}$ by the Zeeman energy $E_{Zeeman} = g\mu_B B$. Here μ_B denotes the Bohr magneton and g the Landé g-factor. Experimentally this splitting manifests as the appearance of additional half integer steps $\frac{N}{2}2e^2/h$. At B = 4T (Figure 2b), we clearly observe Zeeman splitting of the first sub-band, where an additional plateau emerging at 0.5G_0 is coupled with a reduction in the 1G_0 plateau. However, the dispersion of the second plateau is strikingly different. Only a small plateau is visible at 1.5G_0, and the size of the 2G_0 plateau is increased, rather than reduced.

Conductance measurements at zero bias voltage with increasing magnetic field provide further insight into the sub-band dispersions. Figure 3 shows the (a) zero bias conductance and (b) transconductance as a function of magnetic field, together with (c) linecuts of the conductance for increased clarity. As expected, the 0.5G_0 plateau emerges from the 1G_0 plateau at B = 0 T, when E_1 splits into sub bands $E_{1\uparrow}$ and $E_{1\downarrow}$ with applied magnetic field. Both the 0.5G_0 and the 1G_0 plateau remain flat throughout the magnetic field range studied. In contrast, the second plateau at 2G_0 increases in height for magnetic fields larger than 400 mT almost reaching 3G_0 at 2 T. A clearer plateau at 2G_0 emerges at B = 0.5 T and increases linearly in width with a g-factor similar to the 0.5G_0 plateau. We believe that this effect can only be explained by a near-degeneracy of the E_2 and E_3 states for increasing magnetic field, where the plateau at 2G_0 originates from the levels $E_{2\uparrow}$ and $E_{3\uparrow}$, while the plateau at 3G_0 originates from the levels $E_{2\downarrow}$ and $E_{3\downarrow}$. This near-degeneracy persists up to a magnetic field of 3 T where the 1.5G_0 plateau emerges, when $E_{2\uparrow}$ separates from $E_{3\uparrow}$. We convert the plateau width to energy from the individual gate traces by using the lever arm η extracted from Figure 2. This way we can directly extract the sub-band spacing $E_{2\uparrow} - E_{1\uparrow}$ and the individual g-factors g_1, $g_{2,3}$ through a linear fit fixed at the origin to $E_{1\downarrow} - E_{1\uparrow}$ and $E_{2\downarrow,3\downarrow} - E_{2\uparrow,3\uparrow}$ (Figure 3d,e). For $g_{2,3}$ we only fit the range up to 3 T beyond which $E_{2\uparrow}$ and $E_{3\uparrow}$ no longer split together and find g_1 = 39 ± 1, $g_{2,3}$ = 38 ± 1 as well as a constant sub-band spacing $E_{2\uparrow} - E_{1\uparrow} \approx 16$ meV.

Orbital degeneracy of sub-bands has previously been observed in metallic point contacts[29] and recently also in passivated narrow InAs nanowires with highly symmetric conducting channels.[27] However, the magnetoconductance of InSb nanowires may deviate significantly from the results found in InAs nanowires. In InAs, Fermi level pinning leads to conduction close to the nanowire surface,[31,32] which strongly influences the sub-band dispersion in magnetic field.[33,34] InSb has no surface accumulation,[35] and the electron wave function will be more strongly confined in the center of the nanowire. For cylindrical nanowires individual sub-band wave functions are given by Bessel functions with different orbital angular momentum along the wire (Figure 4a), and numerical simulations of wires with a hexagonal cross-section show qualitatively similar results.[28,36]

An additional magnetic field will add Zeeman splitting, but also can contribute to orbital effects, which can substantially change the sub-band dispersion depending on the orientation of the field with respect to the nanowire axis.[37] Numerical simulations of nanowires have shown that orbital effects can dominate over Zeeman effects in the sub-band dispersion, leading to a decrease of the energy splitting between E_2 and E_3 for a perpendicular magnetic field.[37] As the sub-band dispersion determines the phase diagram for MZMs, understanding the

DOI: 10.1021/acs.nanolett.6b00051
Nano Lett. 2016, 16, 3482–3486

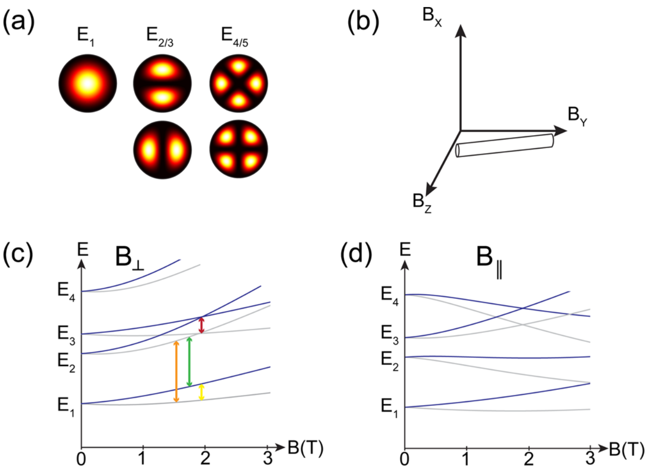

Figure 4. (a) Probability density of the first five sub-bands of a cylindrical nanowire. (b) Orientation of the nanowire with respect to the magnetic field axes. (c,d) Numerical simulations of the sub-band dispersion of a InSb nanowire in perpendicular (c) and parallel (d) magnetic field. The levels $E_{n\uparrow}$ are drawn in gray and $E_{n\downarrow}$ in blue.

role of orbital effects in these nanowires is crucial for interpreting phase diagram measurements. We use the model presented in ref 37 together with the parameters of our device (wire radius: 35 nm; g-factor: 40) to simulate this change in the sub-band dispersion for a magnetic field perpendicular (Figure 4c) and parallel (Figure 4d) to the nanowire. A perpendicular magnetic field causes all four sub-bands $E_{2\uparrow\downarrow}$ and $E_{3\uparrow\downarrow}$ to shift higher in energy, decreasing their energy splitting for increasing magnetic field, until the levels cross. In contrast, a parallel magnetic field increases the energy splitting of $E_{2\uparrow\downarrow}$ and $E_{3\uparrow\downarrow}$ due to their different orbital angular momentum. While the simulations shown in Figure 4c do not perfectly match the experimental data presented in Figure 3a,b, as they show crossings of $E_{2,3\uparrow\downarrow}$ instead of an extended degeneracy, their qualitative behavior for differing orientations of magnetic field supports our interpretation of the data in terms of orbital effects.

We further confirm our interpretation of orbital effects by measuring the transconductance for differing orientations of magnetic field with respect to the nanowire axis, as shown in Figure 5. For magnetic fields orientated perpendicular to the nanowire, either along B_Z (Figure 5a,b), or B_X (Figure 5c,d), a splitting is resolved at the beginning of the first plateau marking the onset of the 0.5 plateau at B = 0.6 T. However, both magnetic field directions show a transition directly from 1G_0 to 2G_0 across this magnetic field range, with no visible 1.5G_0 plateau. However, for the magnetic field aligned along B_Y (mostly parallel to the nanowire) shown in Figure 5e,f, we do see a clear difference. Now two new plateaus emerge almost simultaneously around $B_Z \approx 0.75$ T, with the second plateau at 1.5 and not at 2G_0, in agreement with the results of the numerical simulations in Figure 4. The clear difference between parallel and perpendicular orientations is in agreement with our interpretation of the role of orbital effects in modifying the sub-band dispersions in these nanowires.

In conclusion we achieved substantial improvements in electrical transport measurements of InSb nanowires by using a high quality hBN dielectric and clearly demonstrated conductance quantization at zero magnetic field, as well the role of orbital effects in determining the behavior of energy sub-bands. Further investigation is required to resolve the

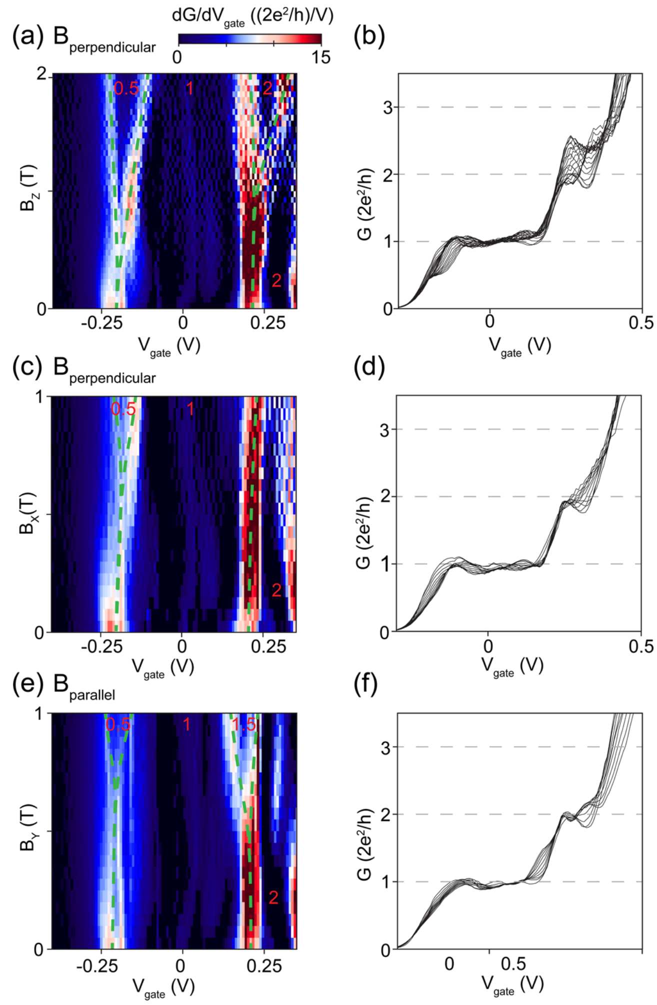

Figure 5. Transconductance dG/dV_{gate} and differential conductance G for three different directions of the magnetic field all taken at V_{bias} = 0 mV. Green dashed lines indicating the sub-band spacing in (a,c,e) are drawn as guide to the eye, and red numbers label the height of the conductance plateaus. B_Z is increased from 0−2 T and $B_{X,Y}$ from 0−1 T. (a,b) Magnetic field aligned along B_Z and (c,d) B_X, both perpendicular to the nanowire. (e,f) Magnetic field aligned along B_Y, parallel to the nanowire.

differences between the numerical simulations of orbital effects and experimental data at low magnetic fields, which may result from an unusual modification of the sub-band states under electrostatic gating due to the strong SOI in these nanowires. In the future these technical improvements will allow the more detailed investigation of features in the first plateau, such as signatures of a helical gap,[38,39] or the presence of a 0.7 anomaly.[40−42] The large SOI in our InSb nanowire strongly influences the electron dispersion relation, and the tunability with magnetic field could add new insight into the underlying physics.[43] We did not see any clear features related to the 0.7 anomaly in our devices. However, in other material systems the 0.7 state becomes more pronounced at higher temperatures,[40] and our devices were only studied at 20 mK. A more detailed study of the temperature dependence of conductance quantization may reveal more information about the existence of this intriguing state in nanowire QPCs.

DOI: 10.1021/acs.nanolett.6b00051
Nano Lett. 2016, 16, 3482−3486

■ ASSOCIATED CONTENT

Supporting Information

The Supporting Information is available free of charge on the ACS Publications website at DOI: 10.1021/acs.nanolett.6b00051.

Detailed fabrication recipe, a discussion of the subtracted series resistance, and additional data of the main device as well as data of QPC devices fabricated with a SiO_2 dielectric (PDF)

■ AUTHOR INFORMATION

Corresponding Author

*E-mail: l.p.kouwenhoven@tudelft.nl.

Present Address

[§]CNRS-Laboratoire d'Analyze et d'Architecture des Systemes (LAAS), Université de Toulouse, 7 avenue du Colonel Roche, F-31400 Toulouse, France.

Notes

The authors declare no competing financial interest.

■ ACKNOWLEDGMENTS

The authors thank M. Wimmer, P. Kim, and A. Akhmerov for helpful discussions, S. Goswami for help with the hBN transfer, and D. van Woerkom for help with nanowire deposition. This work has been supported by funding from the Marie Curie ITN S[3]Nano, the ERC starting grant STATOPINS 638760, NWO/FOM, and Microsoft Corporation Station Q.

■ REFERENCES

(1) Nadj-Perge, S.; Frolov, S. M.; Bakkers, E. P. A. M.; Kouwenhoven, L. P. *Nature* **2010**, *468*, 1084−1087.

(2) Van den Berg, J. W. G.; Nadj-Perge, S.; Pribiag, V. S.; Plissard, S. R.; Bakkers, E. P. A. M.; Frolov, S. M.; Kouwenhoven, L. P. *Phys. Rev. Lett.* **2013**, *110*, 066806.

(3) Petersson, K. D.; McFaul, L. W.; Schroer, M. D.; Jung, M.; Taylor, J. M.; Houck, A. A.; Petta, J. R. *Nature* **2012**, *490*, 380−383.

(4) Liang, D.; Gao, X. P. *Nano Lett.* **2012**, *12*, 3263−3267.

(5) Rossella, F.; Bertoni, A.; Ercolani, D.; Rontani, M.; Sorba, L.; Beltram, F.; Roddaro, S. *Nat. Nanotechnol.* **2014**, *9*, 997−1001.

(6) Žutić, I.; Fabian, J.; Das Sarma, S. *Rev. Mod. Phys.* **2004**, *76*, 323−410.

(7) Hofstetter, L.; Csonka, S.; Nygård, J.; Schönenberger, C. *Nature* **2009**, *461*, 960−963.

(8) Das, A.; Ronen, Y.; Heiblum, M.; Mahalu, D.; Kretinin, A. V.; Shtrikman, H. *Nat. Commun.* **2012**, *3*, 1165.

(9) Mourik, V.; Zuo, K.; Frolov, S. M.; Plissard, S. R.; Bakkers, E. P. A. M.; Kouwenhoven, L. P. *Science* **2012**, *336*, 1003−1007.

(10) Deng, M. T.; Yu, C. L.; Huang, G. Y.; Larsson, M.; Caroff, P.; Xu, H. Q. *Nano Lett.* **2012**, *12*, 6414−6419.

(11) Churchill, H. O. H.; Fatemi, V.; Grove-Rasmussen, K.; Deng, M. T.; Caroff, P.; Xu, H. Q.; Marcus, C. M. *Phys. Rev. B: Condens. Matter Mater. Phys.* **2013**, *87*, 241401.

(12) Deng, M.; Yu, C.; Huang, G.; Larsson, M.; Caroff, P.; Xu, H. *Sci. Rep.* **2014**, *4*, 7261.

(13) Lutchyn, R. M.; Stanescu, T. D.; Das Sarma, S. *Phys. Rev. Lett.* **2011**, *106*, 127001.

(14) van Wees, B. J.; van Houten, H.; Beenakker, C. W. J.; Williamson, J. G.; Kouwenhoven, L. P.; van der Marel, D.; Foxon, C. T. *Phys. Rev. Lett.* **1988**, *60*, 848−850.

(15) Wharam, D. A.; Thornton, T. J.; Newbury, R.; Pepper, M.; Ahmed, H.; Frost, J. E. F.; Hasko, D. G.; Peacock, D. C.; Ritchie, D. A.; Jones, G. A. C. *J. Phys. C: Solid State Phys.* **1988**, *21*, L209.

(16) Chou, H. T.; Lüscher, S.; Goldhaber-Gordon, D.; Manfra, M. J.; Sergent, A. M.; West, K. W.; Molnar, R. J. *Appl. Phys. Lett.* **2005**, *86*, 073108.

(17) Többen, D.; Wharam, D. A.; Abstreiter, G.; Kotthaus, J. P.; Schaffler, F. *Semicond. Sci. Technol.* **1995**, *10*, 711.

(18) Koester, S. J.; Brar, B.; Bolognesi, C. R.; Caine, E. J.; Patlach, A.; Hu, E. L.; Kroemer, H.; Rooks, M. J. *Phys. Rev. B: Condens. Matter Mater. Phys.* **1996**, *53*, 13063−13073.

(19) van Weperen, I.; Plissard, S. R.; Bakkers, E. P. A. M.; Frolov, S. M.; Kouwenhoven, L. P. *Nano Lett.* **2012**, *13*, 387−391.

(20) Gül, Ö; van Woerkom, D. J.; van Weperen, I.; Car, D.; Plissard, S. R.; Bakkers, E. P. A. M.; Kouwenhoven, L. P. *Nanotechnology* **2015**, *26*, 215202.

(21) Dean, C.; Young, A.; Meric, I.; Lee, C.; Wang, L.; Sorgenfrei, S.; Watanabe, K.; Taniguchi, T.; Kim, P.; Shepard, K.; Hone, J. *Nat. Nanotechnol.* **2010**, *5*, 722−726.

(22) Castellanos-Gomez, A.; Buscema, M.; Molenaar, R.; Singh, V.; Janssen, L.; van der Zant, H. S. J.; Steele, G. A. *2D Mater.* **2014**, *1*, 011002.

(23) Plissard, S. R.; Slapak, D. R.; Verheijen, M. A.; Hocevar, M.; Immink, G. W. G.; van Weperen, I.; Nadj-Perge, S.; Frolov, S. M.; Kouwenhoven, L. P.; Bakkers, E. P. A. M. *Nano Lett.* **2012**, *12*, 1794−1798.

(24) Car, D.; Wang, J.; Verheijen, M. A.; Bakkers, E. P. A. M.; Plissard, S. R. *Adv. Mater.* **2014**, *26*, 4875−4879.

(25) Flöhr, K.; Liebmann, M.; Sladek, K.; Günel, H. Y.; Frielinghaus, R.; Haas, F.; Meyer, C.; Hardtdegen, H.; Schäpers, T.; Grützmacher, D.; Morgenstern, M. *Rev. Sci. Instrum.* **2011**, *82*, 113705.

(26) Suyatin, D. B.; Thelander, C.; Björk, M. T.; Maximov, I.; Samuelson, L. *Nanotechnology* **2007**, *18*, 105307.

(27) Ford, A.; Kumar, S. B.; Kapadia, R.; Guo, J.; Javey, A. *Nano Lett.* **2012**, *12*, 1340.

(28) van Weperen, I. Ph.D. thesis, TU Delft, 2014.

(29) Krans, J. M.; Van Ruitenbeek, J. M.; Fisun, V. V.; Yanson, I. K.; De Jongh, L. J. *Nature* **1995**, *375*, 767−769.

(30) Kouwenhoven, L. P.; van Wees, B. J.; Harmans, C. J. P. M.; Williamson, J. G.; van Houten, H.; Beenakker, C. W. J.; Foxon, C. T.; Harris, J. J. *Phys. Rev. B: Condens. Matter Mater. Phys.* **1989**, *39*, 8040−8043.

(31) Scheffler, M.; Nadj-Perge, S.; Kouwenhoven, L. P.; Borgström, M. T.; Bakkers, E. P. A. M. *J. Appl. Phys.* **2009**, *106*, 124303.

(32) Halpern, E.; Elias, G.; Kretinin, A. V.; Shtrikman, H.; Rosenwaks, Y. *Appl. Phys. Lett.* **2012**, *100*, 262105.

(33) Holloway, G. W.; Shiri, D.; Haapamaki, C. M.; Willick, K.; Watson, G.; LaPierre, R. R.; Baugh, J. *Phys. Rev. B: Condens. Matter Mater. Phys.* **2015**, *91*, 045422.

(34) Tserkovnyak, Y.; Halperin, B. I. *Phys. Rev. B: Condens. Matter Mater. Phys.* **2006**, *74*, 245327.

(35) King, P. D. C.; Veal, T. D.; Lowe, M. J.; McConville, C. F. *J. Appl. Phys.* **2008**, *104*, 083709.

(36) Vuik, A.; Eeltink, D.; Akhmerov, A. R.; Wimmer, M. *arXiv:1511.08044*, 2015. http://iopscience.iop.org/article/10.1088/1367-2630/18/3/033013/meta.

(37) Nijholt, B.; Akhmerov, A. R. *arXiv:1509.02675*, 2015.

(38) Středa, P.; Šeba, P. *Phys. Rev. Lett.* **2003**, *90*, 256601.

(39) Pershin, Y. V.; Nesteroff, J. A.; Privman, V. *Phys. Rev. B: Condens. Matter Mater. Phys.* **2004**, *69*, 121306.

(40) Thomas, K. J.; Nicholls, J. T.; Simmons, M. Y.; Pepper, M.; Mace, D. R.; Ritchie, D. A. *Phys. Rev. Lett.* **1996**, *77*, 135−138.

(41) Bauer, F.; Heyder, J.; Schubert, E.; Borowsky, D.; Taubert, D.; Bruognolo, B.; Schuh, D.; Wegscheider, W.; von Delft, J.; Ludwig, S. *Nature* **2013**, *501*, 73−78.

(42) Iqbal, M. J.; Levy, R.; Koop, E. J.; Dekker, J. B.; De Jong, J. P.; van der Velde, J. H. M.; Reuter, D.; Wieck, A. D.; Aguado, R.; Meir, Y.; van der Wal, C. H. *Nature* **2013**, *501*, 79−83.

(43) Goulko, O.; Bauer, F.; Heyder, J.; von Delft, J. *Phys. Rev. Lett.* **2014**, *113*, 266402.

DOI: 10.1021/acs.nanolett.6b00051
Nano Lett. 2016, 16, 3482−3486